Surasani etal2013

DATASET · MAY 2014

READS
31

6 AUTHORS, INCLUDING:

Li Li
Pennsylvania State University
73 PUBLICATIONS **662** CITATIONS
SEE PROFILE

Jonathan Ajo-Franklin
Lawrence Berkeley National Laboratory
85 PUBLICATIONS **472** CITATIONS
SEE PROFILE

Susan Sharpess Hubbard
Lawrence Berkeley National Laboratory
248 PUBLICATIONS **3,390** CITATIONS
SEE PROFILE

Yuxin Wu
University of California, Berkeley
50 PUBLICATIONS **336** CITATIONS
SEE PROFILE

energy&fuels

Article

pubs.acs.org/EF

Bioclogging and Permeability Alteration by *L. mesenteroides* in a Sandstone Reservoir: A Reactive Transport Modeling Study

Vikranth K. Surasani,[†,‡] Li Li,[*,†] Jonathan B. Ajo-Franklin,[§] Chris Hubbard,[§] Susan S. Hubbard,[§] and Yuxin Wu[§]

[†]John and Willie Leone Family Department of Energy and Mineral Engineering, The Pennsylvania State University, University Park, Pennsylvania, United States

[‡]Department of Chemical Engineering, Birla Institute of Science and Technology, Pilani-Hyderabad Campus, Hyderabad, Andhra Pradesh, India

[§]Earth Science Division, Lawrence Berkeley National Laboratory, Berkeley, California, United States

ABSTRACT: Selective bioclogging targets the biofilm growth in highly permeable zones of reservoirs or aquifers to divert water into low permeability zones. It alters the hydrodynamics of the subsurface flow systems to favorable performance conditions. Applications may include microbial-enhanced-hydrocarbon-recovery (MEHR) and bioremediation. Despite its success at the laboratory scale, application of bioclogging at the reservoir scale is hindered by the lack of understanding and advanced modeling and prediction tools. To understand controls of bioclogging processes at the reservoir scale, a Reactive Transport Model (RTM) has been developed in this work for in situ biostimulation of *L. mesenteroides*. This fermenting bacterium produces the biopolymer dextran in the presence of sucrose. As a first step, we considered the flow, transport, and bacterial growth and dextran production reactions in a single phase fluid (water) system, because most reactions occur either in the water phase or at the water−solid interface. Parameters for biomass growth and dextran production were obtained from column experimental data. The numerical experiments were carried out using the spatial distribution of porosity and permeability extracted from open-hole well logs collected at a characterization well near the King Island gas field in Southern Sacramento basin in California. The numerical experiments suggest that there exists an optimum range of injection rates (between 543 and 1,195 bbls/day). The volumetric injection rates need to be sufficiently fast to overcome microbial growth and clogging at the vicinity of the bore wells. They also need to be low enough to allow sufficiently long residence times for dextran production. Results show significant dextran formation and the associated porosity and permeability alterations to divert water into low permeability zones. The bioclogging effectiveness, measured by the percentage of the water diverted into the low permeability zones, varied between 10 to 75% depending on injection conditions. With the same total mass injection rates of sucrose, increasing flow rate is more effective in selectively bioclogging highly permeable zones than increasing sucrose concentration. Other processes, including the attachment of biomass to the solid surface without being washed out, are also important. The developed model offers a powerful tool to optimize injection conditions for effective bioclogging in naturally heterogeneous reservoirs.

1. INTRODUCTION

Biofilms typically consist of a matrix of extracellular polymeric substance (EPS) and bacterial cells, the production of which leads to the reduction in porosity and permeability in porous media. This phenomenon is often referred to as the bioclogging process. Conventionally, bioclogging has been the focus of many studies due to its detrimental impacts on process units such as heat exchangers, medical implants, and well bores. Literature on bioclogging over the past decade suggests that the preferential bioclogging has become a viable technique in many applications such as bioremediation[1] and Microbial-Enhanced-Hydrocarbon-Recovery (MEHR).[2] During water flooding in secondary recovery, hydrocarbons in highly permeable zones are preferentially swept by injected water while those in low permeability zones remain intact. Selective bioclogging, where we choose to selectively clog the highly permeable and oil-depleted zones, is an effective technique to divert water toward the oil rich low permeability zones.[3−5] In bioremediation, bioclogging of aquifer paths can lead to the formation of impermeable biobarriers that inhibit contaminant transport and divert groundwater around the contaminated zone.[6] Despite its promise in applications, bioclogging may lead to detrimental effects due to the uncontrolled growth of biomass near injection wells. In MEHR treatment, it can cause expensive damage to well bores.[7] Uncontrolled bioclogging of preferential paths in an aquifer may also hinder further treatment of contaminants in bioremediation.[8] Success of preferential bioclogging at the reservoir scale depends on fundamental understanding of the coupled flow, transport, and biogeochemical reaction processes. It is also important to identify the controlling parameters during field scale applications.

The effectiveness of bioclogging can be controlled by many factors. Experimental studies have revealed the impact of the flow conditions on bioclogging phenomena. One dimensional column experiments[9−12] showed the development of biofilm near injection ports, which resulted in permeability reduction up to 2 to 3 orders of magnitude. Two dimensional micromodel experiments showed biomass formation as clusters

Received: July 27, 2013
Revised: October 24, 2013

Table 1. Kinetic-Controlled Reactions: Bacteria Growth, Dextran Production, and Immobilization of Biomass Components[a]

reaction index	reactions
E_1: cell growth and enzyme production	$\text{Sucrose} + 0.2NH_4^+ + 0.341HCO_3^- \rightarrow 0.20C_5H_7O_2N_{(w)} + 0.141\text{Fructose} + 0.071\text{Lactate} + 0.071\text{Acetate} + 0.0141\text{Mannitol} + 0.071\text{Ethanol} + 0.418CO_2 + 0.726H_2O + \text{Dextransucrase}$
E_2: dextran production	$5.3\text{Sucrose} + \text{Dextransucrase} \rightarrow 2.0\text{Dextran}_{(w)} + 4.5\text{Fructose} + \text{Dextransucrase}$
E_3: bacterial cell immobilization	$C_5H_7O_2N_{(w)} \leftrightarrow C_5H_7O_2N_{(S)}$
E_4: dextran immobilization	$\text{Dextran}_{(w)} \leftrightarrow \text{Dextran}_{(S)}$

[a]Note that the subscript "w" represents the biomass species that are present in water however not dissolved in water. The subscript "S" represents species that attach to the solid.

and preferential water flow paths exist within the clusters.[6,13,14] Bioclogging experiments in flow cells using more complex flow fields led to the formations of preferential flow patterns.[5,15,16] In most studies, EPS forms the majority of the biomass that causes bioclogging, while the volume of the bacterial cells is negligible compared to EPS.

Over the past decades, substantial research has focused on bacteria and the conditions for the production of EPS that contribute to bioclogging. *Leuconostoc mesenteroides* has been found to effectively produce extracellular polymer substance.[17] Its production can be controlled by using different carbon sources. In the presence of sucrose, it produces dextran, a water-insoluble bioclogging agent. *L. mesenteroides* has been used in a core experiment[18] to produce dextran and have been shown to successfully divert the flow from highly permeable to low permeability zones. Sucrose concentration and flow rates have been found to be important in the plug development and propagation.[19,20] Column experiments also showed that biomass plug and its propagation can be periodic in nature and is associated with the oscillations in pressure drop across the porous media.

Although these studies help identify the important factors that can control bioclogging and permeability alteration, it is important to evaluate reservoir scale feasibility. Field scale studies are typically very expensive. Field MEHR tests have so far mostly focused on in situ production of microbial metabolites such as gases, acids, solvents, and immobile biomass species (e.g., cells and EPS).[21,22] These metabolites alter oil−water interfacial tension (IFT), wettability, and viscosity as well as permeability by selective plugging. The success of these field-scale applications, however, remains ambiguous. One existing augmentation field trial utilized the sucrose metabolism of *L. mesenteroides*.[17] Unfortunately, the results were mixed, possibly due to transport/flushing of the active microbial community.

To understand the reservoir scale feasibility, multiple factors need to be taken into account simultaneously, including the coupling between flow, transport, and microbe-mediated reactions and the operational conditions such as injection condition as well as the physical and chemical heterogeneities.[23−26] In this context, Reactive Transport Models (RTM) can provide powerful tools to understand the transport and fate of biogeochemical reaction products, the associated evolution of the physical properties of the reservoirs, and the effectiveness of the bioclogging process. As a first step toward understanding the bioclogging process at the reservoir scale, a reactive transport model is developed in this work to simulate the coupled flow, transport, and the bacterial growth and dextran production during in situ biostimulation of *L. mesenteroides*. One of our previous studies examined the biostimulation of *L. mesenteroides* in a synthetic carbonate reservoir and the geochemical control of the bioclogging process.[27] In this work, the modeling was carried out for a reservoir based on the King Island gas field in California. The distribution of the porosity and permeability of the field was obtained by utilizing open-hole logging data from a recently drilled scientific characterization well. The reaction network, dextran production kinetics, and petrophysical relationships in this work were validated using previous column-scale bioclogging experiments.[28] Here we conduct the analysis by varying several important operational and biomass growth variables, including the sucrose mass injection rates (sucrose concentration and volumetric injection rates) and *L. mesenteroides* attachment rates. The effectiveness of bioclogging was quantified by the water flooding simulations that measure the percentage of water diversion.

2. REACTIVE TRANSPORT PROCESSES AND MODELING

Bioclogging in porous media involves several processes, including flow and transport of chemical and biological species, the production of the biomass (microbes and EPS, mostly dextran in our case), and the immobilization of biomass as biofilm. In this section, we present the details of microbe-mediated reactions that involve the dextran producing bacteria *L. mesenteroides*, the mathematical representation of the reactions flow processes, and the modeling framework. Kinetic parameters, including those for biomass growth and dextran production, were obtained using bioclogging column experimental data.

2.1. Microbe-Mediated Reactions. *Leuconostoc mesenteroides*, a facultative microbe in the natural environments, has been recognized as a potential applicant for selective plugging in MEHR.[29,30] It is an oxygen-tolerant microbe known for producing EPS in the presence of sucrose as the carbon source.[31] The detailed reactions that lead to dextran production can be complex. Here we present a relatively simplified however representative form of the reaction network that has been developed in our previous work.[27] The reaction network in Table 1 shows a two-step mechanism. The reaction E_1 is the cell growth that produces the bacterial cells $C_5H_7O_2N_{(w)}$ in water and the production of the enzyme Dextransucrase. It was

dx.doi.org/10.1021/ef401446f | Energy Fuels XXXX, XXX, XXX−XXX

Table 2. Mass Conservation Equations of Chemical and Biomass Species in Aqueous Phase

	species	mass conservation
1	sucrose	$\frac{\partial(\varphi C_1)}{\partial t} = \nabla\cdot(\varphi D_1 \nabla C_1) - \nabla(\varphi u C_1) - \nu_{1,1}R_{1,1} - \nu_{1,2}R_{1,2}$ (1)
2	*L. mesenteroides*	$\frac{\partial(\varphi C_2)}{\partial t} = \nabla\cdot(\varphi D_2 \nabla C_2) - \nabla(\varphi u C_2) - \nu_{2,E_1}R_{E_1} - \nu_{2,3}R_{E_3}$ (2)
3	dextran	$\frac{\partial(\varphi C_3)}{\partial t} = \nabla\cdot(\varphi D_3 \nabla C_3) - \nabla(\varphi u C_3) - \nu_{3,E_2}R_{E_2} - \nu_{3,E_4}R_{E_4}$ (3)

derived using the bacterial energetic method[32] where $C_5H_7O_2N$ is a representative chemical formula of the bacterial cell. According to bacterial energetics, some fraction of the electron transfer is utilized for energy production and the remaining fraction is utilized for cell growth. In deriving the reaction network we assumed a fraction of 0.4 for cell growth and the rest for energy reaction.[33] The reaction E_2 represents the catalytic conversion of sucrose into fructose and dextran induced by the enzyme dextransucrase.

The biomass includes both the bacterial cell and the produced dextran. The bacterial cells can attach to the solid phase and therefore can exist in both aqueous and solid phases. Dextran has a relatively low solubility and typically exists in solid form.[34] However, under flow conditions, immobilized dextran can detach and transport in insoluble form. In this study, biofilm refers to the immobile biomass on solid phases that include bacterial cells and dextran, both of which contribute to bioclogging and permeability modification. The immobilization of biomass can be represented with reactions E_3 and E_4. In these reactions, $C_5H_7O_2N_{(w)}$ and $C_5H_7O_2N_{(S)}$ represent bacterial cells in the water and solid phases, respectively. $Dextran_{(w)}$ and $Dextran_{(S)}$ represent dextran in the water and solid phases, respectively.

In addition to these reactions that form the driving force of the system, a series of speciation reactions occur in the aqueous phase and are typically considered as instantaneous reactions.[35−37] These reactions are commonly present in water and can be very important for bioclogging in formations such as carbonate reservoirs.[27] In this work, however, these aqueous reactions are not as important in influencing the bioclogging processes due to the general nonreactive nature of the sandstone. Please also note that for the same reason we have ignored the major cations such as Ca(II) and Mg(II) in this work.

2.2. Reactive Transport Processes and Equations. In addition to the microbe-mediated reactions, the selective bioclogging processes also involve injection of fluid into the subsurface and the flow and transport of multiple chemical and biological species. Reactive Transport Modeling was used to integrate multiple physical (flow and transport), chemical, and biological processes, as shown in the equations in Table 2. Here eqs 1 to 3 are the mass conservation equations for an aqueous primary species i with fractional pore volume (porosity φ) and aqueous concentration C_i (mol/L). The symbol ν_{iE_k} is the stoichiometric coefficient of species i in microbe-mediated reaction E_k with rate R_{E_k} (mol/L/s). The symbol D_i (m^2/s) is the dispersion/diffusion coefficient of the species, and u (m/s) is the superficial velocity. The dispersive and advective transport depends on the flow field that determines the fate of the influent species reaching the reactive zones and the biomass accumulation. The Fickian diffusion coefficient for sucrose in water is assumed to be 5.19×10^{-6} cm^2/s, with a typical tortuosity value of 0.6 to take into the effects of porous media on diffusion coefficient in porous media.[38] The longitudinal dispersion coefficient (α_L) and transverse dispersion coefficient (α_T) were taken as 15 and 1.5 cm, respectively.[39] The quasi-stationary flow field for pressure and gravity driven flow was represented by Darcy's law.[40]

Here the equations were solved using the reactive transport code CrunchFlow. CrunchFlow has been widely applied in various applications,[41−45] including those that involve microbe-mediated reactions.[25,26] The growth rate depends on the amount of biomass (eq 4) and immobilization depends on available pore surface area (eq 5), as will be discussed later in the reaction kinetics section. Flow and diffusive transport within the biofilm were neglected so the biomass matrix was assumed to be impermeable. The code solves the mass conservation equations.

2.3. Reaction Kinetics. *2.3.1. Biomass growth.* The growth of biomass was assumed to follow the Monod rate law.[32,46] The rates of the two microbe-mediated reactions E_1 and E_2 were represented as

$$R_i = k_{\max,i} X_i \frac{C_{Su}}{C_{Su} + K_{M,Su,i}} \quad (4)$$

Here R_i is the cell growth rate and the enzyme production rate for reactions E_1 and E_2, respectively. The rates depend on the maximum rate constant k_{max} (mol/L/cells/s), the amount of immobile biomass component X_i, the half-saturation constant $K_{M,Su,i}$, and the sucrose concentration C_{Su} (mol/L). For example, in reaction E_2 the enzyme-mediated dextran production rate R_2 depends on $k_{max,2}$ and the amount of enzyme X_2.[47] The molar volume of the cell biomass was assumed to be 336 cm^3/mol, a number in the middle range of reported values.[48] Similar to other works,[49] it was assumed that one *L. mesenteroides* cell produces one unit of enzyme dextransucrase per mole of sucrose metabolized.

2.3.2. Immobilization of Biomass. The amount of immobilized biomass depends on the attachment and detachment processes. Attachment is the process of forming immobile biomass from their respective mobile species, the rate of which is directly proportional to the aqueous concentrations of biomass species and is typically expressed with first-order expression from the filtration theory[50,51] for bacterial and EPS to the soliddeposition. Likewise, detachment is the process of forming the mobile biomass from immobile phase. Its rate is directly proportional to the amount of biomass present in the solid phase and is similarly expressed with first-order kinetics based on the shear forces or sloughing processes.[52] These constants are functions of many parameters such as flow velocity, viscosity and density of aqueous phase, grain size of the biomass particles, and many more empirical parameters.[15] However, there is no unified approach that quantitatively

dx.doi.org/10.1021/ef401446f | Energy Fuels XXXX, XXX, XXX−XXX

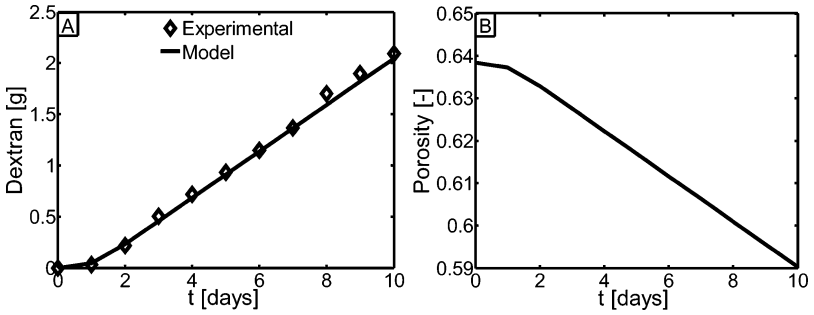

Figure 1. A) Comparison of data from bioclogging column experiments (symbols) and reactive transport modeling output (line) for dextran production and B) corresponding model prediction of porosity evolution.[28]

describes these processes. Here we assumed that the rates of E_3 and E_4 in units of mol/s take the following form

$$R = k_a A\left(1 - \frac{C_w}{K_{eq}}\right) \tag{5}$$

where C_w denotes the concentration of biomass species in the water phase, and the K_{eq} values are essentially the thermodynamics limit or the maximum concentration of biomass species that can exist in the water phase. These values were taken as 10^{-6} M for reaction E_3 (L. *mesenteroides*) and 10^{-15} M for dextran based on literature values.[30,34,53] Dextran is largely known as insoluble,[30] while bacterial cells can exist in water without attaching to the solid phase. The k_a (mol/m^2/s) is the kinetic rate constant, and A denotes the bulk surface area (m^2) of immobile biomass. In essence, the biomass can exist in both the water and solid phases, with the rates of attachment and detachment following the above equation.

2.4. Porosity and Permeability Update. The conservation of solid phase biomass in terms of volumetric porosity can be estimated using the differential equation

$$\frac{d\varphi}{dt} = \nu_{i,E_3} R_{E_3} \frac{\tilde{M}_i}{\rho_i} + \nu_{i,E_4} R_{E_4} \frac{\tilde{M}_i}{\rho_i} \tag{6}$$

where $\tilde{M}_i$ is the molar weight (kg/mol) of the solid phases i, and ρ_i is the mass density (kg/m^3) of the solid phase i. Efforts have been made to correlate permeability with biomass using analytical models[54−56] and pore network models.[5,16] However, few theoretically derived correlations exist to relate the change in permeability to the amount of biomass in the porous media. Existing relationships are mostly empirical.[10,14,57] As a result, we adopted the widely accepted power-law relation that describes the filtration of fine particles into the porous media.[55] This is consistent with the assumption of impermeable biofilm in the following form:

$$\kappa = \kappa_0\left(\frac{\varphi}{\varphi_0}\right)^3 \tag{7}$$

Here κ and κ_0 are the permeability values at certain time t and at the initial time, respectively. Similarly, the reactive surface is an important parameter and was updated using the porosity values based on the geometric of spherical particles:[58]

$$A_S = A_{s,0}\left(\frac{\varphi}{\varphi_0}\right)^{2/3} \tag{8}$$

The exponent 2/3 was used because area depends on particle radius raised to a power of 2, while porosity corresponds to volume change with dependence on particle radius raised to a power of 3.

2.5. Biomass Growth and Dextran Production Parameters from Column Experiments. The developed model includes a large number of parameters, including the growth and production kinetics of bacteria and dextran. These parameters were obtained by matching the model with data from column experiments inoculated with the bacterium *L. mesenteroides* and the sucrose growth media.[28] The bacterium was allowed to grow and produce dextran for 10 days with fresh sucrose media supplied once every day. The column was monitored for the dextran production and associated geophysical measurement such as resistivity and phase, which indicates changes in the petrophysical properties of the column.

A reactive transport model was set up using one-dimensional computational domain that consists of 100 grid blocks. The goal was to obtain the key parameters that characterize the bacterial growth and dextran production. Ten cycles of substrate injection and dextran production were conducted in the model to exactly represent the bioclogging experiment. In each cycle the substrate was injected into the column for 1 h, and the column was allowed to produce dextran for 23 h under no flow conditions. The simulation results were used to match the dextran, total organic carbon, as well as geophysical measurement data by adjusting the rate constant of biomass growth and dextran production. Figure 1A shows the experimental data and the predicted evolution of dextran production are consistent. The corresponding predicted average porosity evolution is shown in Figure 1B. For the best match, the rate constants k_{max} for cell growth reaction E_1 and enzyme catalyzed reaction in E_2 are 2.07×10^{-17} and 3.60×10^{-12} mol/L/cell/s, respectively. The half saturations $K_{M,Su}$ in eq 4 for reactions E_1 and E_2 are 7.3×10^{-3} and 7.3×10^{-4} mol/L, respectively, which are among typical values in the literature.[59,60]

3. BIOCLOGGING SIMULATION OVERVIEW

3.1. Reservoir Simulation Domain and Bioclogging Scheme. The synthetic simulation domain has a dipping layered structure based on logs recently collected as part of the scientific characterization effort at the King Island gas field, Sacramento Basin, CA. The well (Citizen Green #1) was drilled as part of a CO_2 sequestration project. The extensive open-hole logging suite provided an excellent source of petrophysical data. The field, while not an MEHR target, has structure representative of potential target fields farther south in the oil-rich San Joaquin Basin. The horizon examined in this study

dx.doi.org/10.1021/ef401446f | *Energy Fuels* XXXX, XXX, XXX−XXX

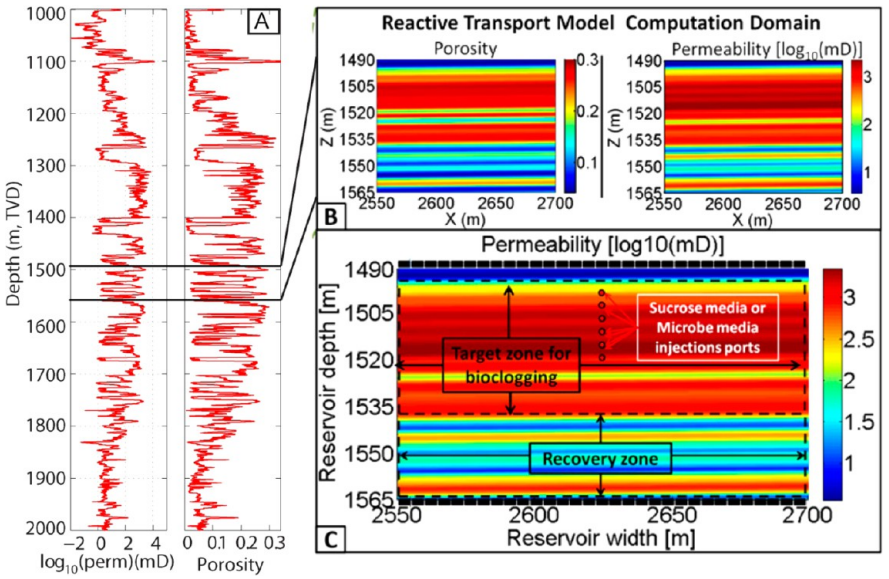

Figure 2. Distribution of porosity and permeability in the simulation domain extracted from nuclear magnetic resonance logging data in King Island gas field located in the Sacramento Basin, CA. A) Porosity and permeability, B) derived two-dimensional distribution of porosity and permeability in a segment of the reservoir for the target simulation domain, and C) basic bioclogging treatment representation on reservoir formation showing target zone, recovery zone, and media injection ports.

Table 3. Variables of Simulation Cases

parameter	values						
TVIR: $\dot{q}_{tot}$ [bbls/day][a] (with C_{Su} = 1.47 mol/L, $\log_{10}(k_{a,E_3})$ = −13.0 mol/m^2/s)	543	706	869	1032	1195		
sucrose injection concn: C_{Su} [mol/L] ($\dot{q}_{tot}$ = 1195 bbls/day, $\log_{10}(k_{a,E_3})$ = −13.0 mol/m^2/s)	0.1	0.25	0.5	0.75	1.0	1.25	1.47
kinetic rate constant: $\log_{10}(k_{a,E_3})$ [mol/m^2/s] ($\dot{q}_{tot}$ = 1195 bbls/day, C_{Su} =1.47 mol/L)	−14.2	−13.8	−13.4	−13.0			

[a]TVIR stands for Total Volumetric Injection Rates (TVIR); bbls stands for "barrels". It is a widely used field unit used in the field of petroleum engineering. 1 bbl = 0.159 m^3.

is the top section of the Mokelumne River Formation, permeable fluvial sandstone with interbedded silt and clay stones. High permeability sections of the unit average over 3 Darcy, while the siltier sections are often submilli Darcy (mD). In this work, the high permeability regions correspond to areas which would be swept early in water flooding, while the siltier regions are typical of zones with a high residual oil fraction. For the flow modeling effort, both porosity and permeability were extracted from nuclear magnetic resonance logging data by extruding a slightly smoothed version of the log estimated porosity and permeability along the regional dip (1.5 degrees). The logs were vertically smoothed with a 5 point running mean filter before transformation into the model.

The size of the two-dimensional computation domain is 150 m × 75 m as shown in Figure 2B. This size is about the typical size of the "influencing zone" of one injection well at the typical injection rates of several hundreds to over a thousand meters in water flooding and secondary oil recovery practices.[61,62] Each grid block is 0.25 m in depth and 1 m in width. The total number of grid blocks is 45,000. The synthetic treatment strategy is shown in Figure 2C. Based on the permeability data, the computation domain is classified into two sections: the highly permeable target zone for bioclogging and the low permeability recovery zone. Six injection ports were placed in the highly permeable zone at 2625 m in x direction and from 1502.5 to 1515 m in the depth direction. The sucrose media was evenly distributed and injected into the formation through the six points representative of well perforations. Compared to the flow field that was driven by the sucrose media injection, the background flow in the reservoir is negligible. The left and right boundaries of computation domain were set as open boundaries. No flow conditions were applied at the top and bottom boundaries in the z direction.

Many factors can affect the effectiveness of bioclogging treatments, including the presence of microbe that produce bioclogging agents, the total mass injection concentration of sucrose, and the injection rates. Bioclogging can also be influenced by the attachment and detachment kinetics,[51,63,64] i.e. the ability of aqueous microbes and dextran to form biofilm on the formation surface. In this work, we present a series of numerical bioclogging experiments by systematically changing one parameter at a time, as shown in Table 3. The total volumetric injection rates (TVIR) were chosen to be in the typical range from 543 to 1195 bbls/day that are within the typical injection rates during water flooding in secondary oil recovery.[61,62] The sucrose concentrations were chosen to be between 0.10 and 1.47 mol/L. Kinetic rate constants were tested in the range of $10^{-14.2}$ to 10^{-13} mol/m^2/s. The goal was to understand the coupled processes and identify the key parameters that control the effectiveness of bioclogging.

3.2. Water Flooding Test: Quantification of Bioclogging Effectiveness. The goal of selectively bioclogging the high permeability zone is to divert more water into the original low permeability recovery zone during enhanced oil recovery. Here we use a numerical water flooding test to quantify the effectiveness of the bioclogging by comparing the fractional

dx.doi.org/10.1021/ef401446f | Energy Fuels XXXX, XXX, XXX−XXX

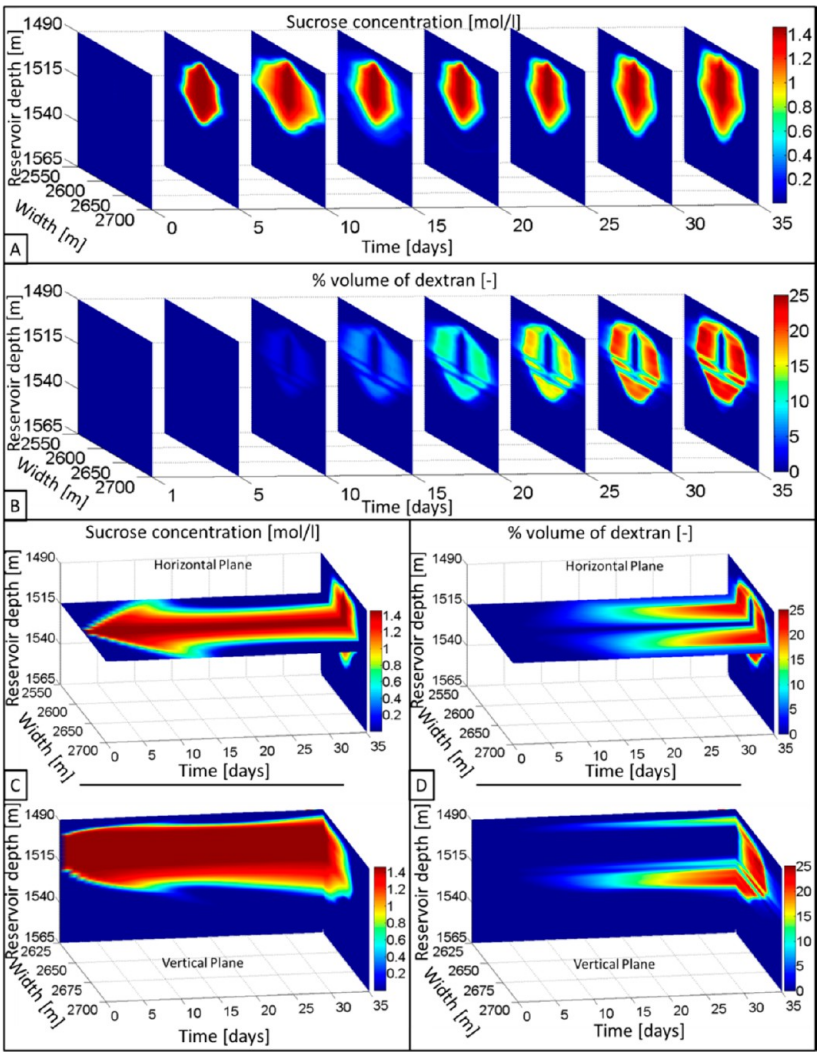

Figure 3. Spatial and temporal evolution of sucrose concentration and percentage dextran volume during bioclogging treatment in the base case scenario. A) Sucrose concentration distribution, B) spatial distribution of dextran percentage volume, C) sucrose concentration on horizontal section at the reservoir depth 1515 m with maximum initial permeability and vertical section at 2625 m where injection ports are located, and D) corresponding percentage dextran production on vertical and horizontal sections.

water that come out of the recovery zone before and after the bioclogging experiment using nonreactive flow and transport modeling. In the simulation, water was injected at a rate of 543 bbls/day through a wellbore across the entire depth of the reservoir. The water will flow through the domain depending on the permeability distribution. The proportion of the water that goes through the originally low permeability recovery zone was quantified and used as a measure of the bioclogging effectiveness. A larger increase in percentage of water from the original low permeability means higher effectiveness. The flooding tests were applied in all cases after 35 days of bioclogging treatment.

4. RESULTS AND DISCUSSION

In this section we first present a base case scenario to show the coupled flow, transport, and reaction processes during bioclogging. The effects of influencing variables, including sucrose concentrations, volumetric injection rates, and bacteria attachment and detachment, were then examined to understand their effects on bioclogging effectiveness.

4.1. Base Case Scenario. The injection conditions for this base case were carried out with a total volumetric injection rate of 543 bbls/day and at the sucrose concentration of 1.47 mol/L with the kinetic attachment rate constant of 10^{-13} mol/m^2/s. The initial microbial community was assumed to be present in the reservoir and to be spatially uniform at a concentration of 10^{-6} % volume. Sucrose solution was continuously injected into the reservoir for 35 days to allow sufficient production of dextran. The spatial and temporal evolution of sucrose concentrations are shown in Figure 3A. Sucrose concentrations are high in areas close to the injection ports in the first 5 days. From day 5 to 10, the concentrations decrease because the sucrose disperses deep into the reservoir with a larger impact area. Between days 10 and 15, the concentrations are reduced due to sucrose consumption during microbial activity. At the end of day 15, most of the sucrose concentration fronts recede toward the injection ports. Starting from day 25, concentrations have again started to increase, particularly in the vertical direction below the perforated interval. This is because at a later stage the porosity has been decreased to a larger extent, which decreases reactive water−solid interface and the overall reaction rates of bacterial growth and dextran production. This sequence

dx.doi.org/10.1021/ef401446f | Energy Fuels XXXX, XXX, XXX−XXX

of concentration perturbations in the reservoir formations are visualized in Figure 3C for the horizontal section at the reservoir depth of 1515 m, which possess maximum initial permeability profile, and the vertical section at the reservoir width of 2625 m.

Similarly, the spatial and temporal evolutions of dextran formation are plotted in Figure 3B. For the first 5 days, dextran formation was negligible. During this period, in the presence of sucrose (reaction E_1), microbes self-replicate to produce bacteria and the enzyme dextransucrase. Between days 5 and 10, bacterial cells and enzyme activity are produced sufficiently to be visible. During this period, sucrose concentrations decrease near the injection ports (Figure 3A). During the period from day 25 to 35, there is rapid dextran formation as concentration fronts surge across the reservoir (compare parts A and B of Figure 3). By the end of bioclogging treatment on day 35, there is a significant increase in dextran volume, occupying a maximum of 24% total volume in the target zone.

Figure 4 illustrates the spatial evolution of porosity and permeability during the bioclogging treatment. Significant

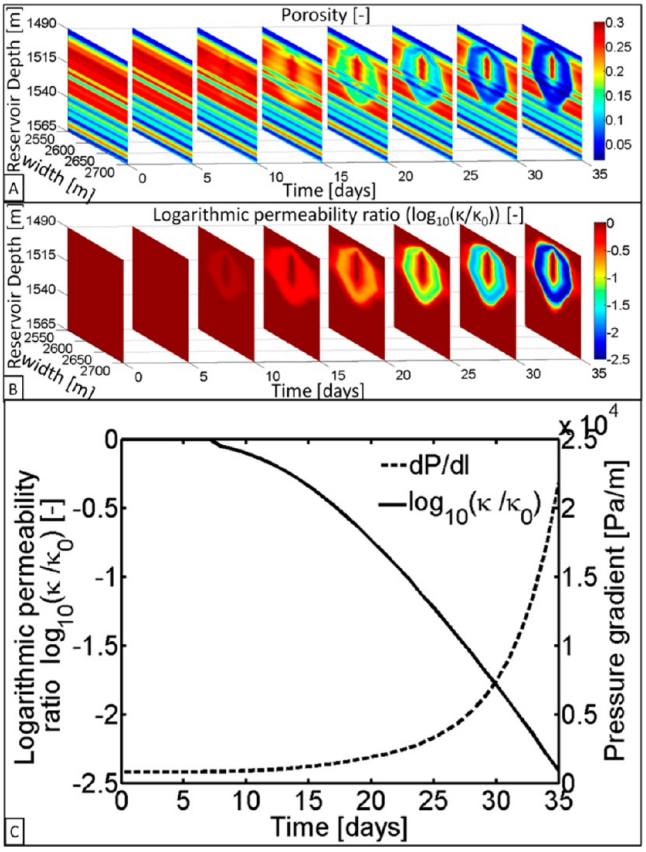

Figure 4. Spatial and temporal evolution of A) porosity, B) logarithmic ratio of permeability k at time t over the initial permeability k_0, and C) evolving permeability ratio and pressure gradient on the horizontal edge at the depth 1515 m shown in Figure 3.

reduction in porosity is observed starting from day 15 (Figure 4A). The corresponding evolution of logarithmic permeability ratio is shown in Figure 4B, with a maximum decrease of 2.5 orders of magnitude. With the intense microbial activity and dextran production, a ringlike bioclogging structure is formed surrounding the perforated injection interval. As the porosity continued to decrease, reduction in pore volume leads to a decrease in water−solid contact area and the sucrose conversion rates. In addition, the porosity decrease also results in the decrease in residence time. The combination of these two leads to the reduction in the total amount of sucrose conversion to dextran. As such, after a critical volume of dextran formation, the sucrose concentration fronts surges in areas of significant reduction in porosity.

To quantify the effectiveness of bioclogging, Figure 4C shows the temporal evolution of pressure gradient and the effective permeability ratio for the horizontal section at the depth 1515 m that was shown in Figure 3C. Pressure gradient was estimated from the injection port to left/right boundary, whereas the logarithmic permeability ratio was calculated from the point on horizontal edge where critical maximum reduction in permeability occurred. Because the injection rates remain constant during the bioclogging treatment, the pressure gradients increase significantly as permeability decreases. Figure 4C shows that permeability started to drop after day 7, consistent with dextran and receding concentration fronts in Figure 3A. In the early stages, especially before day 15, the dextran formation and porosity reduction is relatively slow, leading to negligible pressure gradient. The pressure gradient increases faster when the permeability is reduced to approximately 0.5 orders of magnitude on day 15. After that the permeability decreases exponentially as indicated by the almost linear decrease in logarithmic permeability ratio. The magnitude of the pressure evolution here is similar to the pressure gradient evolution observed in one-dimensional flow conditions by Fogler et al.[18,20]

The hydrodynamic alterations are also quantified using the water flooding test explained in section 2.2. The stream line plots and flooding output velocity profiles in the left and right boundaries are presented in Figure 5 for before and after bioclogging. The bioclogging effectiveness is quantified by the fraction of total injected water coming out of the recovery zone. In the baseline case, all stream lines (white lines on porosity heterogeneity as backdrop) are linear, and water at any depth flows straight toward left and right boundaries. Before the bioclogging, most of the injected water flows through the target bioclogging zone, with only 8% of injected water flowing out of the recovery zone. After the treatment, the stream lines show that the water released in the target zone moves straight near the biologically clogged zone and diverts toward the nearest region of low resistance. Injected water flows into the recovery zone first and then into the unclogged high permeability zone. The velocity profiles at left and right boundaries show significant reduction of flow in the target zone and significant increase in the recovery zone, with 38% of total injected water flowing out of the recovery zone. The bypassing of flow from the bioclogged zone has also been observed in 2D flow cell experiments.[5,65,66]

4.2. Controlling Factors that Determine Bioclogging Effectiveness. Here we use reactive transport modeling to evaluate the sensitivity of the bioclogging effectiveness to various parameters, including the initial biomass distribution, sucrose mass injection rates, and the kinetic rates of attachment and detachment of *L. mesenteroides*.

4.2.1. Dependence on in Situ and ex Situ Microbial Sources. Potentially there are two bacterial sources for bioclogging. One is an in situ bacterial source, where *L. mesenteroides* or a similar strain pre-exists in the reservoir so only the injection of sucrose and nutrients are necessary to stimulate the bacteria. The other is the ex situ or augmentation

dx.doi.org/10.1021/ef401446f | Energy Fuels XXXX, XXX, XXX−XXX

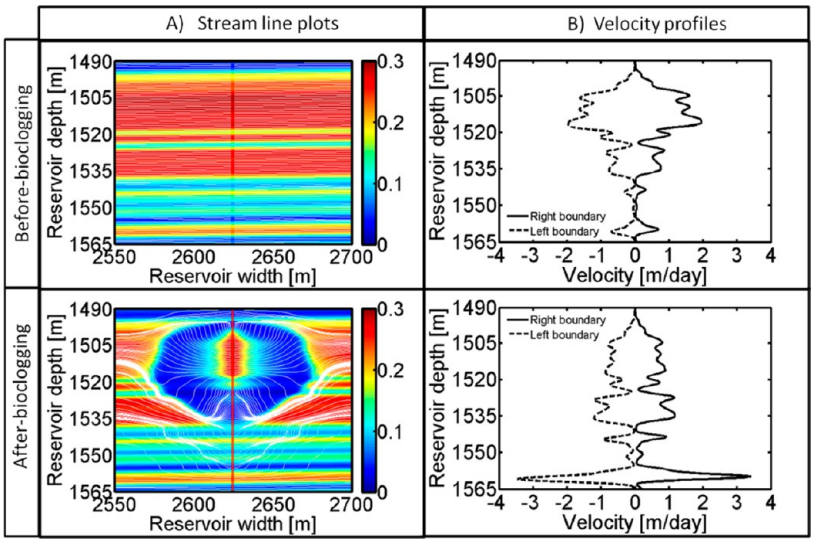

Figure 5. Water flooding test before (top) and after (bottom) bioclogging treatment. A) Stream line plots and B) water velocity profiles at left and right boundaries. Both figures show significant alteration in the flow field.

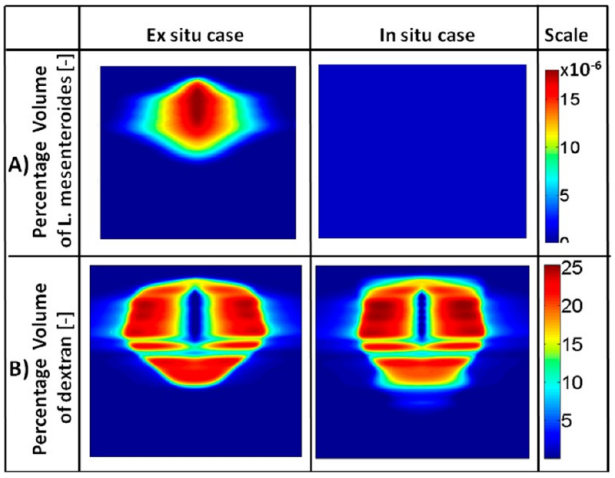

Figure 6. Comparison of the ex situ and in situ cases for A) Left: the initial distribution of percentage volume of microbe after the inoculation process in the ex situ case; Right: in the in situ case, the microbe is assumed to have a uniform distribution of 10^{-6} % of the total volume; B) the spatial distribution of dextran for the ex situ (left) and in situ (right) cases at the end of 35 days of bioclogging treatment, assuming the initial distribution of microbe in A. This figure shows that the initial distribution of the bacteria has negligible effects on the distribution of dextran at the end of bioclogging treatment. The permeability alteration is largely controlled by the transport of sucrose in reservoir after injection.

case, where *L. mesenteroides* initially does not exist in the reservoir and need to be injected as well. These species need to be inoculated in the reservoir before the start of in situ biostimulation. Here we compare the two cases to understand if they affect the spatial distribution of initial bacteria to a level that affect the effectiveness of bioclogging.

For the ex situ case, microbial media containing *L. mesenteroides* at an optimal concentration of 0.13 mol/L were injected before the bioclogging treatment. Injections above this concentration may result in large amounts of bacterial attachments near the perforated interval, which could yield undesirable near well-bore clogging. The volumetric injection rate is kept at 543 bbls/day. The injected bacteria can either attach to the solid phase or flow out of the domain, depending on the attachment and detachment kinetics. Here a kinetic attachment constant of 10^{-13} mol/m^2/s was used.

Predicted microbial distribution on the solid phase after 30 days of microbial injection is plotted in total volume percentage in Figure 6A for ex situ case. Microbial abundance reaches its maximum close to the injection wells and decreases with increasing distance from the injection ports. The initial *L. mesenteroides* distribution in the target zone is 10^{-6} % total volume, which is similar to the initial microbe concentration assumed in the base case scenario for the in situ case. The bioclogging treatment was then carried out using the same injection condition as in the base case scenario, i.e. sucrose concentration C_{Su} of 1.45 M, and total volumetric injection rates of 543 bbls/day. The spatial distributions of the biomass for this ex situ case and the previous in situ case are shown in Figure 6A after 35 days of bioclogging treatment. Comparison of the two cases shows that there are some slight differences in the shape and the maximum values of dextran formation. For example, there is a larger bacteria-free zone close to the perforations in the ex situ case than that in the in situ case. The in situ case also has a slightly larger overall areal extent of the bioclogged zone. However, over time the system is largely driven by the spatial distribution of injected sucrose, which leads to similar spatial distribution of dextran (Figure 6B). These two cases end up having similar bioclogging effectiveness, with water fractions of 0.37 and 0.38 from the recovery zone in the in situ and ex situ cases, respectively. This indicates that the in situ and ex situ cases in general have similar bioclogging outcome when the average initial microbe abundance in the ex situ simulation is similar to the initial uniform distribution of microbe in the in situ case. However, from an economic perspective, the ex situ case does require additional cost for the pretreatment before the bioclogging treatment. A more significant issue is also the survival of any strain added to the subsurface system. With the exception of bioaugmentation for the reductive dechlorination of dense solvents,[67] few successful examples of field-scale augmentation (i.e., ex situ treatments) exist due to the out-competition by the native microbial community.

dx.doi.org/10.1021/ef401446f | *Energy Fuels* XXXX, XXX, XXX–XXX

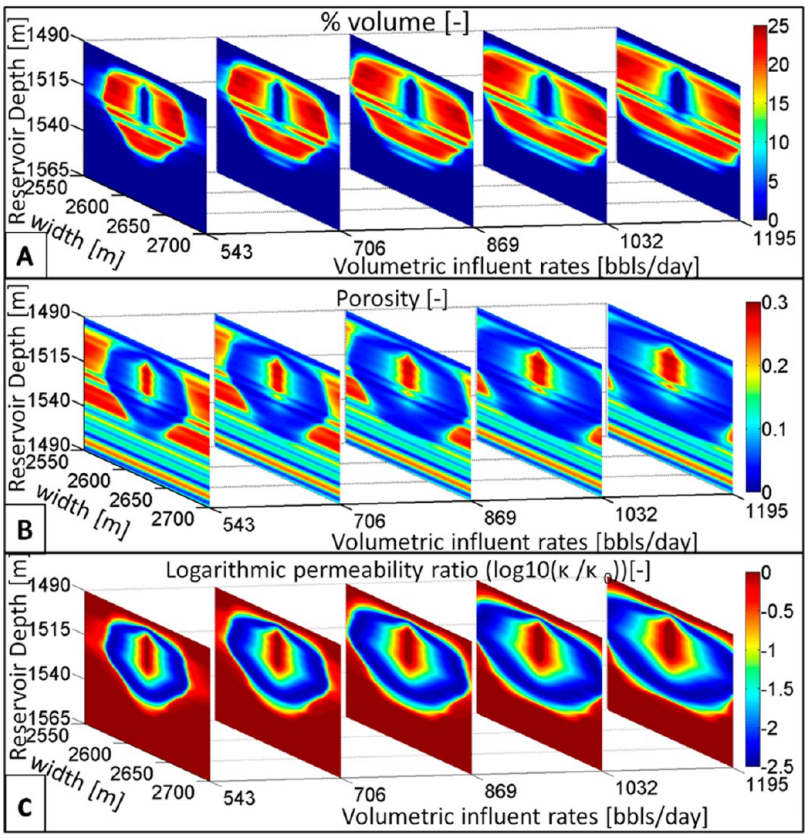

Figure 7. Effects of volumetric injection rates on A) Volume percentage of dextran, B) porosity, and C) permeability ratio profiles after 35 days of bioclogging treatment.

4.2.2. Dependence on Sucrose Mass Injection Rates. An important parameter that can influence permeability modification is the sucrose mass injection rates. Sucrose injection provides the driving force for the bioclogging. The relative rates between the microbial growth, dextran production, and the flow determine the spatial distribution of chemical and biological species in aqueous phase and the accumulation of biomass. In this subsection, we assess the sensitivity of bioclogging effectiveness to the mass injection rates of sucrose. The total mass of sucrose can vary depending on two parameters, sucrose concentrations (C_{Su}) and total volumetric injection rates ($\dot{q}_{tot}$). The initial and operating conditions of the bioclogging simulations are in Table 3 for parameters **TVIR** and **SC**. *L. mesenteroides* was assumed to be present uniformly within the reservoir in all cases. Selection of C_{Su} and $\dot{q}_{tot}$ can be treated as an optimization problem.

We first examine the effects of volumetric injection rates with constant sucrose injection concentration. The total volumetric injection rates vary from 543 to 1195 bbls/day with a constant sucrose concentration of 1.47 M. The spatial profiles of dextran, porosity, and permeability after 35 days of bioclogging treatment are shown in Figure 7. In all 5 cases, dextran occupied a maximum of 24.29% volume. This leads to a maximum decrease in permeability of approximately 2.5 orders of magnitude. The increase in volumetric injection rates leads to two effects. First, it significantly increases the areal extent of dextran formation. With the injection rates of 1195 bbls/day, the clogged area occupies the whole target zone. In the case of 543 bbls/day, the clogged area is about two-thirds of the target zone. Correspondingly, the area of porosity and permeability reduction is also larger with higher injection rates. Second, increasing the injection rates leads to an increasingly large open zone without dextran formation. This is because the increase in volumetric flow rates results in the decrease in the residence time. Near the injection ports, at low residence time, produced enzyme in water is swept away quickly and attaches to the formation farther from injection ports, which leads to the dextran formation far away from the injection ports. If the volumetric injection rate is decreased to a rate lower than 543 bbls/day, the treatment will lead to significant clogging at the vicinity of the wellbore, which is not desirable.

The water flooding tests are applied for all five cases after 35 days of bioclogging treatment. Figure 8 represents the stream line plots and the fractional flow out of the recovery zone as a measure of the bioclogging effectiveness. With relatively low volumetric injection rates, injected water manages to flow out through the original high permeability zone due to the relative small clogged zones, resulting in fractional flow rates from the recover zone being 0.38, 0.5, and 0.59. In the case of high volumetric injection rates (1032 and 1195 bbls/day), the bioclogged area is much wider so that most of the injected water is confined to the recovery zone, resulting in fractional flows of 0.69 and 0.75, respectively.

The effect of sucrose injection concentration on bioclogging was evaluated with the sucrose concentrations varying from 0.1 to 1.47 M at the constant volumetric injection rate of 1195 bbls/day. The volume percentage of dextran formation, porosity, and permeability at day 35 of the bioclogging treatment is shown in Figure 9. Increasing inlet sucrose concentration leads to increasing bioclogged areal extent and magnitude. The maximum dextran volume varies from 5% volume in the lowest sucrose concentration case (0.1 M) to

dx.doi.org/10.1021/ef401446f | *Energy Fuels* XXXX, XXX, XXX–XXX

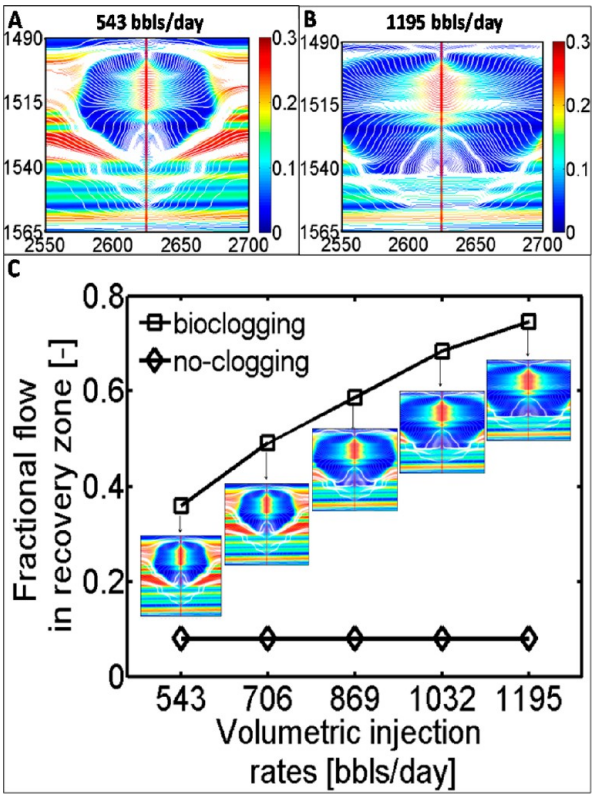

Figure 8. Hydrodynamic alteration and the effectiveness of the bioclogging treatment under different volumetric injection conditions. Streamline plots for the volumetric injection rates A) 543 bbls/day and B) 1195 bbls/day and C) fractional flow in recovery zone as a function of volumetric injection rates. Fractional flow is defined as the fraction of the injected water flowing out of the recovery zone (the original low permeability target zone).

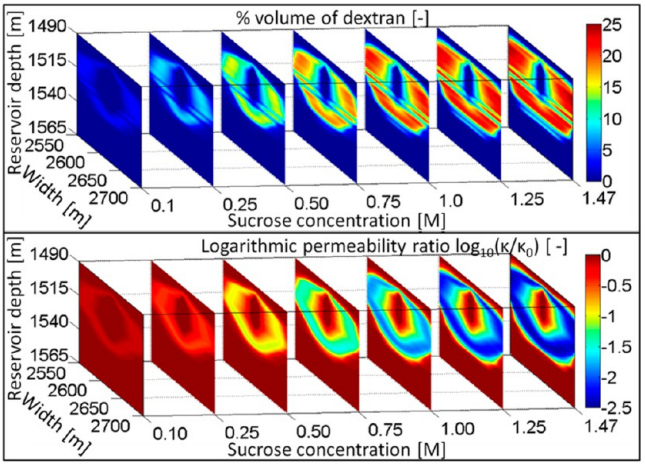

Figure 9. Effects of inlet sucrose concentration on Percentage volume of dextran (top), (bottom) permeability ratio profiles after 35 days of bioclogging treatment with a volumetric injection rate of 1195 bbls/day.

24.7% volume in the highest sucrose concentration case (1.47 M). At constant volumetric injection rates, *L. mesenteroides* and dextransucrase activity (reaction E_1 and E_2) depends on the sucrose concentration (C_{Su}) for the dextran production. The maximum reduction in permeability varies from 0.5 to 2.47 orders of magnitude for the corresponding sucrose concentrations of 0.1 mol/L and 1.47 mol/L, respectively.

The fractional flows from the recovery zones during the water flooding test were plotted as a function of the sucrose mass injection rates in Figure 10. The fraction flow is 0.08 in the no-clogging condition, while varies it from 0.1 to 0.75 for all the stimulated cases. In general, increasing mass injection rates, whether volumetric injection rates or sucrose concentration, leads to an increase in the effectiveness of bioclogging. Figure 10 also shows that with the same mass injection rates, increasing the volumetric injection rate is more effective than increasing the sucrose concentration. For example, at 60 kkg/day of mass injection rates, the top line has the fraction flow of close to 50%, while the bottom line reaches about 38%. The two curves overlap at a high mass injection rate of 97 kkg/day and at the low mass injection rates of 38 kkg/day. Below 38 kkg/day (injection of 543 bbls/day at 1.47 mol/L, or 1195 bbls/day at 0.50 mol/L), if the injection rate is lower than 543 bbls/day, the bioclogging treatment leads to significant clogging at the wellbore, and the treatment is not effective. Because the primary cost of bioclogging treatments is feedstock cost, Figure 10 can be easily translated into units of dollars per day, thus allowing a comparison of recovery improvements as a function of invested assets. Depending on the resource value, this approach could allow direct integration of RTM into biotreatment decisions.

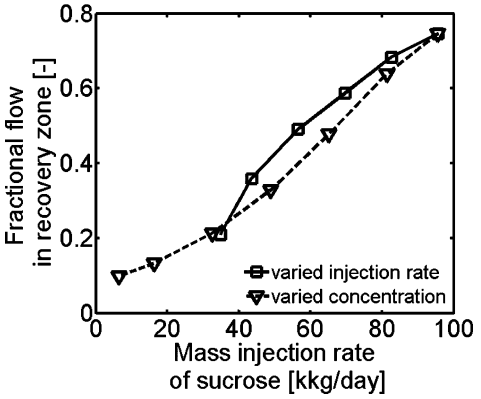

Figure 10. Fractional flow in recovery zone as a function of mass injection rates (varying volumetric flow rates and sucrose concentration). For mass injection rate varying between 40 and 95 kkg/day, increasing volumetric injection rate is more effective than increasing sucrose concentration.

4.2.3. L. mesenteroides Attachment and Detachment Kinetics. As explained earlier, the biomass immobilization can be important in determining the bioclogging effectiveness. Here the effects of such kinetics are examined by fixing other conditions with sucrose concentration being 1.47 mol/L in the injection media and total volumetric injection rates being 1,195 bbls/day however varying the logarithmic kinetic rate constant ($\log(k_{max,E3})$) of reaction E_3 from −14.2 to −13.0 mol/m^2/s. The value of −13.0 mol/m^2/s is what we obtained from the dextran bioclogging experiment.[28] Below $10^{-14.2}$ (mol/m^2/s) no bacterial attachment leads to negligible bacterial activity. Above 10^{-13} mol/m^2/s most of the *L. mesenteroides* can be immobilized within the pore space and effectively clog regions of the reservoir.

All these cases assumed that *L. mesenteroides* initially exists in the reservoir. The spatial distribution of dextran and the

dx.doi.org/10.1021/ef401446f | *Energy Fuels* XXXX, XXX, XXX−XXX

corresponding porosity and permeability evolutions are shown in Figure 11 for day 35. The increase in the kinetic rate

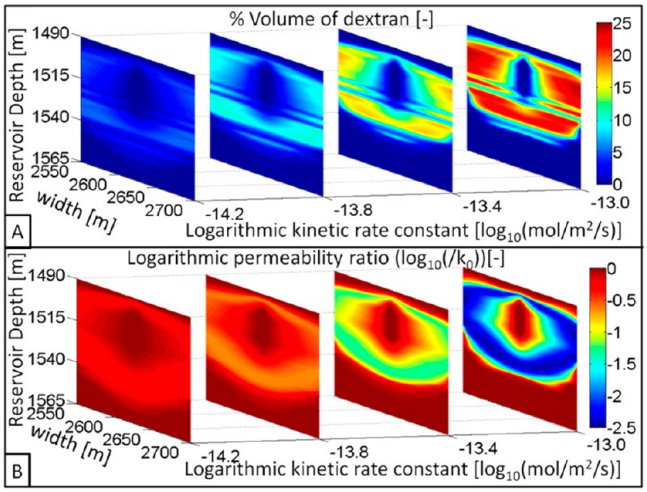

Figure 11. Effects of kinetic rate constant of attachment and detachment A) Percentage volume of dextran, and B) logarithmic permeability ratio profiles after 35 days of bioclogging treatment.

constant $k_{max,E3}$ results in the increase of *L. mesenteroides* concentration on the solid phase. Physically, a higher kinetic rate constant means adhesion of microbes on pore space and higher accumulation rate of biomass on the solid phase without flowing out of the system. The increase in *L. mesenteroides* mass in the immobile biofilm form enhances sucrose conversion to *L. mesenteroides* and dextran because the bacteria in the aqueous form are easily washed away. Figure 12 shows that the

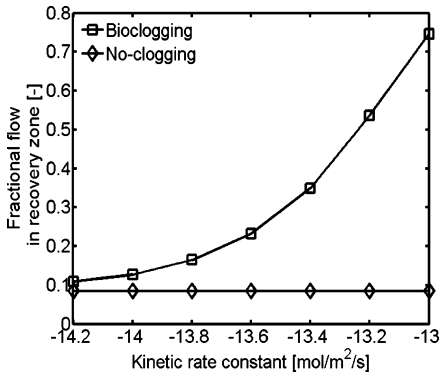

Figure 12. The fractional flow from the recovery zone as a function of *L. mesenteroides* attachment rate constant.

bioclogging effectiveness is sensitive to the attachment kinetics, with the fraction flow increasing from 0.1 to 0.75 with about 1 order of magnitude increase in attachment kinetics.

5. CONCLUSIONS

In this work, we developed a multicomponent reactive transport model for the in situ biostimulation of *L. mesenteroides* at the reservoir scale for the production of a biopolymer dextran to allow the selective bioclogging of highly permeable zones in a realistic reservoir domain. The model explicitly couples flow, transport, and biogeochemical processes during the bioclogging treatment through the injection of sucrose and quantifies the evolution of reservoir properties over time and space. The model was calibrated with kinetic parameters from a column experiment. Numerical bioclogging experiments were carried out with the initial porosity and permeability distribution obtained from a characterization well drilled in the Sacramento Basin. The bioclogging effectiveness was quantified using the water flooding numerical test based on the spatial distribution of porosity and permeability after the bioclogging treatment. As far as we know, these are the first numerical experiments for selective bioclogging at the reservoir scale. This can be important not only for enhanced oil recovery but also for other applications such as bioremediation. This work revealed several interesting aspects of the bioclogging process:

- An optimum volumetric injection rate exists for specific reservoir conditions. The volumetric injection rates must be high enough to overcome the fast growth of *L. mesenteroides* at the vicinity of the injection wells and to achieve bioclogging in an areal extent that is sufficiently large to be effective. The volumetric rates also must be low enough to allow sufficient residence time for the production of the dextran. The magnitude of clogging depends both on the characteristic time scale for biomass production and the residence time, which in turns depend on the size of reservoir. As such, the "effective" range of injection rates from 543 to 1,195 bbls/day is specific to the particular reservoir size in this work and dextran production kinetics. A general "index" type of guideline should be quantified under specific reservoir and bacterial functioning conditions.
- With the same mass injection rates of sucrose, increasing the volumetric injection rate is more effective for bioclogging than increasing the sucrose concentration, because higher volumetric injection rates lead to larger areas of bioclogging in the originally highly permeable zones.
- The success of bioclogging treatment depends largely on the attachment and detachment kinetics of *L. mesenteroides* and the produced dextran on solid phases. If the bacteria or the produced dextran cannot attach to the solid phase fast enough, they tend to be washed out of the reservoir and are not effective in producing the clogging agent dextran. It will be important to understand the conditions that facilitate the attachment of bacteria and dextran on the solid phases and measure these rate constants.

Reactive transport modeling is a powerful integration tool to understand the combined effects of multiple processes that occur simultaneously. Because reservoir scale field treatments are typically very expensive, the numerical experiments offer an economic yet powerful tool for testing various conditions and variables to identify key parameters and processes to optimize bioclogging interventions. The evolving flow heterogeneity caused by bioclogging in multidimensional flow systems is consistent with the observation in two-dimensional flow cell experiments.[5,65] Nonetheless, the presented model has some limitations. First, the simulation neglects flow in the third dimension. The third dimension often has different heterogeneity structures and may show different flow heterogeneity evolutions, particularly in the case of fluvial systems. As such, the 2D simulation may generate idealized bioclogging scenarios that "force" the flow to go into the lateral dimension in contrast to the greater degree of freedom in true field scenarios. The second is the kinetics associated with the attachment and detachment of the biomass, including both bacteria and dextran. These processes play a significant role in determining the success of bioclogging treatment. However, fundamental

dx.doi.org/10.1021/ef401446f | *Energy Fuels* XXXX, XXX, XXX–XXX

understanding and key parameters on the kinetics and thermodynamics of these processes are typically not available. The acquisition of experimental data sets is crucial for the accurate predictions of subsurface reactive transport processes. Such a developed numerical model with more physicochemical representation offers a useful tool for optimizing bioclogging in naturally variable subsurface systems. Third, under natural conditions the microbial community dynamics is much more complicated than what we assume here. For example, here we focus on the pure strain *L. mesenteroides*. Microbial community under reservoir conditions typically is composed of many different strains.[68,69] It is very likely that some other strains can also use sucrose as their carbon source and therefore compete with *L. mesenteroide*, which can affect the survival and kinetics of *L. mesenteroide*.[70,71]

As a result of uncertainties related to fundamental understanding and some key parameters, the presented results also have uncertainties. For example, although dextran and porosity evolution were calculated entirely based on mass conservation, the magnitude change in permeability depends on the porosity-permeability relationship, which tends to be empirical and sensitive to specific conditions. As such, the relationship used may underestimate or overestimate the magnitude of permeability alteration. For any particular reservoirs, it is important to obtain specific porosity-permeability relationship under representative conditions. Nonetheless, the study here shows the promise of using mechanism-based reactive transport modeling to optimize field operation for MEHR.

AUTHOR INFORMATION

Corresponding Author

*Phone: 814-867-3547. Fax: 814-865-3248. E-mail: lili@eme.psu.edu.

Notes

The authors declare no competing financial interest.

ACKNOWLEDGMENTS

The project support from Energy Bioscience Institute (EBI), University of California, Berkeley and the financial support from British Petroleum are gratefully acknowledged. We would also like to thank John H. Beyer and the WESTCARB partnership for allowing use of the Citizen Green #1 well logs for development of our synthetic reservoir model. WESTCARB acquisition of the well logs was supported by the Assistant Secretary for Fossil Energy, Office of Coal and Power Systems through the National Energy Technology Laboratory, of the U.S. Department of Energy, under contract number DE AC0205CH11231.

REFERENCES

(1) Zhang, T. C.; Fu, Y. C.; Bishop, P. L.; Kupferle, M.; Fitzgerald, S.; Jiang, H. H.; Harmer, C. Transport and biodegradation of toxic organics in biofilms. *J. Hazard. Mater.* **1995**, *41* (2−3), 267−285.

(2) Abdel-Waly, A. A. Laboratory study on activating indigenous microorganisms to enhance oil recovery. *J. Can. Pet. Technol.* **1999**, *38* (2), 55−61.

(3) Gullapalli, I. L.; Bae, J. H.; Hejl, K.; Edwards, A. Laboratory design and field implementation of microbial profile modification process. *SPE Reservoir Eval. Eng.* **2000**, *3* (1), 42−49.

(4) Kim, D. S.; Fogler, H. S. Biomass evolution in porous media and its effects on permeability under starvation conditions. *Biotechnol. Bioeng.* **2000**, *69* (1), 47−56.

(5) Thullner, M.; Mauclaire, L.; Schroth, M. H.; Kinzelbach, W.; Zeyer, J. Interaction between water flow and spatial distribution of microbial growth in a two-dimensional flow field in saturated porous media. *J. Contam. Hydrol.* **2002**, *58* (3−4), 169−189.

(6) Baveye, P.; Vandevivere, P.; Delozada, D. Biofilm growth and the related changes in the physical-properties of a porous-medium. 1. Experimental investigation - comment. *Water Resour. Res.* **1992**, *28* (5), 1481−1482.

(7) Brown, L. R. Microbial enhanced oil recovery (MEOR). *Curr. Opin. Microbiol.* **2010**, *13* (3), 316−320.

(8) Baveye, P.; Vandevivere, P.; Hoyle, B. L.; DeLeo, P. C.; de Lozada, D. S. Environmental impact and mechanisms of the biological clogging of saturated soils and aquifer materials. *Crit. Rev. Environ. Sci. Technol.* **1998**, *28* (2), 123−191.

(9) Cunningham, A. B.; Characklis, W. G.; Abedeen, F.; Crawford, D. Influence of biofilm accumulation on porous-media hydrodynamics. *Environ. Sci. Technol.* **1991**, *25* (7), 1305−1311.

(10) Taylor, S. W.; Jaffe, P. R. Biofilm growth and the related changes in the physical-properties of a porous-medium. 1. Experimental investigation. *Water Resour. Res.* **1990**, *26* (9), 2153−2159.

(11) Wu, J. Q.; Gui, S. X.; Stahl, P.; Zhang, R. D. Experimental study on the reduction of soil hydraulic conductivity by enhanced biomass growth. *Soil Sci.* **1997**, *162* (10), 741−748.

(12) Kim, D. S.; Fogler, H. S. The effects of exopolymers on cell morphology and culturability of Leuconostoc mesenteroides during starvation. *Appl. Microbiol. Biotechnol.* **1999**, *52* (6), 839−844.

(13) Vandevivere, P.; Baveye, P. Saturated hydraulic conductivity reduction caused by aerobic-bacteria in sand columns. *Soil Sci. Soc. Am. J.* **1992**, *56* (1), 1−13.

(14) Vandevivere, P.; Baveye, P.; Delozada, D. S.; Deleo, P. Microbial clogging of saturated soils and aquifer materials - evaluation of mathematical-models. *Water Resour. Res.* **1995**, *31* (9), 2173−2180.

(15) Thullner, M. Comparison of bioclogging effects in saturated porous media within one- and two-dimensional flow systems. *Ecol. Eng.* **2010**, *36* (2), 176−196.

(16) Thullner, M.; Zeyer, J.; Kinzelbach, W. Influence of microbial growth on hydraulic properties of pore networks. *Transp. Porous Media* **2002**, *49* (1), 99−122.

(17) Jack, T. R.; Diblasio, E.; Ward, V. Bacterial systems for selective plugging in secondary oil production. *Abstr. Pap. Am. Chem. Soc.* **1983**, *185* (MAR), 3−PETR.

(18) Lappan, R. E.; Fogler, H. S. Reduction of porous media permeability from in situ Leuconostoc mesenteroides growth and dextran production. *Biotechnol. Bioeng.* **1996**, *50* (1), 6−15.

(19) Stewart, T. L.; Fogler, H. S. Biomass plug development and propagation in porous media. *Biotechnol. Bioeng.* **2001**, *72* (3), 353−363.

(20) Stewart, T. L.; Fogler, H. S. Pore-scale investigation of biomass plug development and propagation in porous media. *Biotechnol. Bioeng.* **2002**, *77* (5), 577−588.

(21) Lazar, I. Microbial systems for enhancement of oil recovery used in Romanian oil fields. *Miner. Process. Extr. Metall. Rev.* **1998**, *19* (1), 379−393.

(22) Lazar, I.; Petrisor, I. G.; Yen, T. F. Microbial enhanced oil recovery (MEOR). *Pet Sci. Technol.* **2007**, *25* (11), 1353−1366.

(23) Scheibe, T. D.; Fang, Y.; Murray, C. J.; Roden, E. E.; Chen, J.; Chien, Y.-J.; Brooks, S. C.; Hubbard, S. S., Transport and biogeochemical reaction of metals in a physically and chemically heterogeneous aquifer. *Geosphere* **2006**, *2*, (4), doi: 10.1130/GES00029.1.

(24) Scheibe, T. D.; Hubbard, S. S.; Onstott, T. C.; DeFlaun, M. F. Lessons learned from bacterial transport research at the south oyster site. *Ground Water* **2011**, *49* (5), 745−763.

(25) Li, L.; Gawande, N.; Kowalsky, M. B.; Steefel, C. I.; Hubbard, S. S. Physicochemical heterogeneity controls on uranium bioreduction rates at the field scale. *Environ. Sci. Technol.* **2011**, *45* (23), 9959−66.

(26) Li, L.; Steefel, C. I.; Kowalsky, M. B.; Englert, A.; Hubbard, S. S. Effects of physical and geochemical heterogeneities on mineral transformation and biomass accumulation during a biostimulation experiment at Rifle, Colorado. *J. Contam. Hydrol.* **2010**, *112* (1−4), 45−63.

(27) Vilcáez, J.; Li, L.; Wu, D.; Hubbard, S. S. Reactive transport modeling of induced selective plugging by leuconostoc mesenteroides in carbonate formations. *Geomicrobiol. J.* **2013**, DOI: 10.1080/01490451.2013.774074.
(28) Wu, Y.; Surasani, V. K.; Li, L.; Hubbard, S. S. Geophysical monitoring and reactive transport simulations of bioclogging processes induced by leuconostoc mesenteroides. *Geophysics* **2013**, in press.
(29) Lappan, R. E.; Fogler, H. S. *Leuconostoc mesenteroides* growth kinetics with application to bacterial profile modification. *Biotechnol. Bioeng.* **1994**, *43*, 865−873.
(30) Padmanabhan, P. A.; Kim, D. S. Production of insoluble dextran using cell-bound dextransucrase of *Leuconostoc mesenteroides* NRRL B-523. *Carbohydr. Res.* **2002**, *337*, 1529−1533.
(31) Naessens, M.; Cerdobbel, A.; Soetaert, W.; Vandamme, E. J. Leuconostoc dextransucrase and dextran: production, properties and applications. *J. Chem. Technol. Biotechnol.* **2005**, *80*, 845−860.
(32) Rittmann, B. E.; McCarty, P. L. *Environmental Biotechnology: Principles and Applications*; McGraw-Hill: New York, 2001.
(33) VanBriesen, J. M. Evaluation of methods to predict bacterial yield using thermodynamics. *Biodegradation* **2002**, *13* (3), 171−190.
(34) Jeanes, A.; Haynes, W. C.; Wilham, C. A.; Rankin, J. C.; Melvin, E. H.; Austin, M. J.; Cluskey, J. E.; Fisher, B. E.; Tsuchiya, H. M.; Rist, C. E. Characterization and classification of dextrans from 96 strains of bacteria. *J. Am. Chem. Soc.* **1954**, *76* (20), 5041−5052.
(35) Li, L.; Peters, C. A.; Celia, M. A. Upscaling geochemical reaction rates using pore-scale network modeling. *Adv. Water Resour.* **2006**, *29* (9), 1351−1370.
(36) Morel, F.; Hering, J. G. *Principles and Applications of Aquatic Chemistry*; Wiley: New York, 1993; p xv, 588.
(37) Lichtner, P. C. Continuum model for simultaneous chemical-reactions and mass-transport in hydrothermal systems. *Geochim. Cosmochim. Acta* **1985**, *49* (3), 779−800.
(38) Mair, R. W.; Hurlimann, M. D.; Sen, P. N.; Schwartz, L. M.; Patz, S.; Walsworth, R. L. Tortuosity measurement and the effects of finite pulse widths on xenon gas diffusion NMR studies of porous media. *Magn. Reson. Imaging* **2001**, *19* (3−4), 345−351.
(39) Gelhar, L. W.; Welty, C.; Rehfeldt, K. R. A critical-review of data on field-scale dispersion in aquifers. *Water Resour. Res.* **1992**, *28* (7), 1955−1974.
(40) Dullien, F. A. L. *Porous Media: Fluid Transport and Pore Structure*; Academic Press, Inc.: San Diego, 1991.
(41) Singha, K.; Li, L.; Day-Lewis, F. D.; Regberg, A. B. Quantifying solute transport processes: Are chemically ″conservative″ tracers electrically conservative? *Geophysics* **2011**, *76* (1), F53−F63.
(42) Steefel, C. I.; Lasaga, A. C. A coupled model for transport of multiple chemical species and kinetic precipitation/dissolution reactions with application to reactive flow in single phase hydrothermal systems. *Am. J. Sci.* **1994**, *294*, 529−592.
(43) Li, L.; Steefel, C. I.; Yang, L. Scale dependence of mineral dissolution rates within single pores and fractures. *Geochim. Cosmochim. Acta* **2008**, *72* (2), 360−377.
(44) Salehikhoo, F.; Li, L.; Brantley, S. L. Magnesite dissolution rates at different spatial scales: The role of mineral spatial distribution and flow velocity. *Geochim. Cosmochim. Acta* **2013**, *108* (0), 91−106.
(45) Brunet, J. L.; Li, L.; Karpyn, Z. T.; Kutchko, B.; Strazisar, B.; Bromhal, G. Dynamic evolution of compositional and transport properties under conditions relevant to geological carbon sequestration. *Energy Fuels* **2013**, *27* (8), 4208−4220.
(46) Monod, J. The growth of bacterial cultures. *Annu. Rev. Microbiol.* **1949**, *3*, 371−394.
(47) Neely, W. B. Studies on the enzyme dextransucrase. I. The effect of pH on enzyme activity. *J. Am. Chem. Soc.* **1958**, *80* (8), 2010−2013.
(48) Loferer-Krossbacher, M.; Klima, J.; Psenner, R. Determination of bacterial cell dry mass by transmission electron microscopy and densitometric image analysis. *Appl. Environ. Microbiol.* **1998**, *64* (2), 688−694.
(49) Dols, M.; Remaud-Simeon, M.; Willemot, R. M.; Vignon, M.; Monsan, P. Characterization of the different dextransucrase activities excreted in glucose, fructose, or sucrose medium by Leuconostoc mesenteroides NRRL B-1299. *Appl. Environ. Microbiol.* **1998**, *64* (4), 1298−1302.
(50) Omelia, C. R. Particle particle interactions in aquatic systems. *Colloids Surf.* **1989**, *39* (1−3), 255−271.
(51) Martin, R. E.; Bouwer, E. J.; Hanna, L. M. Application of clean-bed filtration theory to bacterial deposition in porous-media. *Environ. Sci. Technol.* **1992**, *26* (5), 1053−1058.
(52) Clement, T. P.; Peyton, B. M.; Skeen, R. S.; Jennings, D. A.; Petersen, J. N. Microbial growth and transport in porous media under denitrification conditions: Experiments and simulations. *J. Contam. Hydrol.* **1997**, *24* (3−4), 269−285.
(53) Naessens, M.; Cerdobbel, A.; Soetaert, W.; Vandamme, E. J. Leuconostoc dextransucrase and dextran: production, properties and applications. *J. Chem. Technol. Biotechnol.* **2005**, *80* (8), 845−860.
(54) Taylor, S. W.; Milly, P. C. D.; Jaffe, P. R. Biofilm growth and the related changes in the physical-properties of a porous-medium. 2. Permeability. *Water Resour. Res.* **1990**, *26* (9), 2161−2169.
(55) Clement, T. P.; Hooker, B. S.; Skeen, R. S. Macroscopic models for predicting changes in saturated porous media properties caused by microbial growth. *Ground Water* **1996**, *34* (5), 934−942.
(56) Seki, K.; Miyazaki, T. A mathematical model for biological clogging of uniform porous media. *Water Resour. Res.* **2001**, *37* (12), 2995−2999.
(57) Seifert, D.; Engesgaard, P. Sand box experiments with bioclogging of porous media: Hydraulic conductivity reductions. *J. Contam. Hydrol.* **2012**, *136*, 1−9.
(58) Lasaga, A. C. Chemical kinetics of water-rock interactions. *J. Geophys. Res.* **1984**, *89* (B6), 4009−4025.
(59) Jung, J.; Hyun, S. P.; Lee, J. K.; Cho, Y. H.; Hahn, P. S. Adsorption of UO_2^{2+} on natural composite materials. *J. Radioanal. Nucl. Chem.* **1999**, *242* (2), 405−412.
(60) Liu, C.; Kota, S.; Zachara, J. M.; Fredrickson, J. K.; Brinkman, C. K. Kinetic analysis of the bacterial reduction of goethite. *Environ. Sci. Technol.* **2001**, *35* (12), 2482−2490.
(61) Emberley, S.; Hutcheon, I.; Shevalier, M.; Durocher, K.; Gunter, W. D.; Perkins, E. H. Geochemical monitoring of fluid-rock interaction and CO2 storage at the Weyburn CO2-injection enhanced oil recovery site, Saskatchewan, Canada. *Energy* **2004**, *29* (9−10), 1393−1401.
(62) Fathi, S. J.; Austad, T.; Strand, S. Water-based enhanced oil recovery (EOR) by ″smart water″: Optimal ionic composition for EOR in carbonates. *Energy Fuels* **2011**, *25* (11), 5173−5179.
(63) Harvey, R. W.; Garabedian, S. P. Use of colloid filtration theory in modeling movement of bacteria through a contaminated sandy aquifer. *Environ. Sci. Technol.* **1991**, *25* (1), 178−185.
(64) Hornberger, G. M.; Mills, A. L.; Herman, J. S. Bacterial transport in porous-media - evaluation of a model using laboratory observations. *Water Resour. Res.* **1992**, *28* (3), 915−923.
(65) Kildsgaard, J.; Engesgaard, P. Tracer tests and image analysis of biological clogging in a two-dimensional sandbox experiment. *Ground Water Monit. Rem.* **2002**, *22* (2), 60−67.
(66) Sharp, R. R.; Cunningham, A. B.; Komlos, J.; Billmayer, J. Observation of thick biofilm accumulation and structure in porous media and corresponding hydrodynamic and mass transfer effects. *Water Sci. Technol.* **1999**, *39* (7), 195−201.
(67) Damgaard, I.; Bjerg, P. L.; Jacobsen, C. S.; Tsitonaki, A.; Kerrn-Jespersen, H.; Broholm, M. M. Performance of full-scale enhanced reductive dechlorination in clay till. *Ground Water Monit. Rem.* **2013**, *33* (1), 48−61.
(68) Dar, S. A.; Kleerebezem, R.; Stams, A. J. M.; Kuenen, J. G.; Muyzer, G. Competition and coexistence of sulfate-reducing bacteria, acetogens and methanogens in a lab-scale anaerobic bioreactor as affected by changing substrate to sulfate ratio. *Appl. Microbiol. Biotechnol.* **2008**, *78* (6), 1045−1055.
(69) Dunn, R. M.; Mikola, J.; Bol, R.; Bardgett, R. D. Influence of microbial activity on plant-microbial competition for organic and inorganic nitrogen. *Plant Soil* **2006**, *289* (1−2), 321−334.
(70) Atteia, O.; Guillot, C. Factors controlling BTEX and chlorinated solvents plume length under natural attenuation conditions. *J. Contam. Hydrol.* **2007**, *90* (1−2), 81−104.

(71) Waul, C.; Arvin, E.; Schmidt, J. E. Modelling the competitive effect of ammonium oxidizers and heterotrophs on the degradation of MTBE in a packed bed reactor. *Water Res.* **2008**, *42* (12), 3098−3108.